Dynamic Switching Control of Power-Split Hybrid Electric Vehicles Based on Time Delay Prediction and Interference Compensation

Jiajia Wang, Ruochen Wang, Renkai Ding, Qingzhen Han, and Wenhan Yang

***Abstract*—The deterioration of vehicle dynamics caused by the simultaneous action of time delay and interference is a key issue for the switching control system in a power-split hybrid electric vehicle (PS-HEV). This article presents an innovative compound control method based on extended state observer (ESO) incorporating time delay during the mode transition process. First, the coupling effect of time-varying delay and external disturbance during the typical mode switching process is analyzed in depth, and the double deterioration mechanism of the two coupling effects on vehicle dynamics and ride comfort is revealed. To accurately estimate the system disturbance under the influence of time delay, an unconventional ESO is designed further by adopting the Markov chain time delay prediction model, and the main tool for interference observation is selected by comparing the practicability, reachable bandwidth, and observation accuracy. Moreover, the stable mode switching performance and interference suppression are thoroughly investigated, and the smooth transmission of multipower is realized through the multimodule fusion design of the compound coordinated controller. Finally, the hardware-in-the-loop test is implemented to validate the effectiveness of the control strategy, which also provides a novel idea and lays a theoretical foundation for the optimal design of the PS-HEV controller.**

***Index Terms*—Coordinated control, external disturbances, mode transition, power-split hybrid electric vehicle, time-varying delay.**

I. Introduction

HYBRID electric vehicles [1], [2], [3], as one of the important development routes of new energy vehicles, have the key advantages of large cruising range and strong power. Due to the addition of the electric drive system, the engine operating point could be effectively adjusted, which greatly reduces the fuel consumption and pollutant emissions. Among them, power-split hybrid electric vehicle (PS-HEV) could distribute the engine power through the planetary gear set for battery charging or direct driving of the vehicle [4]. It not only decouples the torque and speed of the engine, but also has the function of electronic continuously variable transmission [5]. Since there is no transmission device that loses system energy such as friction belts in traditional mechanical continuously variable transmissions, it also has the advantages of high transmission efficiency and large torque bearing capacity, which has successfully attracted extensive attention from domestic and foreign automakers and researchers [6].

The dynamic switching control of hybrid electric vehicles [7] is mainly aimed at the torque changes coordination of each power source in the mode switching process to reduce the output torque fluctuation of the power coupling mechanism, improve the switching smoothness, and achieve better switching quality [8]. Based on the obvious response gap between engine and motor, the motor torque is usually used to compensate for the problem that the engine cannot be fully controlled to reduce the torque fluctuation [9], [10]. However, the most studies are all based on the parallel or some single-axis hybrid structures, and their torque and speed coupling characteristics of the key components are linear. Then, the corresponding coordinated control design is relatively simple, so extensive and in-depth research results have been obtained [11]. While the PS-HEV often uses multiple planetary gears as its power coupling device, which makes the internal dynamics quite complicated, and the resulting coordination control problem is full of challenges.

In order to solve the jerk problem caused by the start-stop of the engine during the mode switching process of the PS-HEV, Zhao et al. [12] proposed an optimal control strategy for engine shutdown, and used the dynamic programming algorithm to design the optimal towing speed trajectory. Zhu et al. [13] designed four fuzzy PID dynamic regulators in the switching process of the PS-HEV with a single motor. Chen and Hwang [14] focused on the coupling characteristics of the planetary transmission system, and raised a method to effectively reduce the torque fluctuation of the output shaft during the engine start-up process.

It is worth noting that the switching control strategy of PS-HEV proposed in the above research is mostly based on the assumption that the torque control process is ideal and real-time. However, the actual control system of a hybrid vehicle is a typical distributed control system [15]. There are many delays in the

Manuscript received 18 October 2022; revised 16 February 2023; accepted 11 April 2023. Date of publication 20 April 2023; date of current version 22 September 2023. This work was supported by the National Natural Science Foundation of China under Grant 51975253. Recommended for publication by Associate Editor S. Williamson. *(Corresponding author: Jiajia Wang.)*

Jiajia Wang, Qingzhen Han, and Wenhan Yang are with the School of Mechanical Engineering, Yangzhou University, Yangzhou 225000, China (e-mail: wjj751772554@yzu.edu.cn; hanqzh@yzu.edu.cn; whyang@yzu.edu.cn).

Ruochen Wang and Renkai Ding are with the Automotive Engineering Research Institute, Jiangsu University, Zhenjiang 212000, China (e-mail: wrc@ujs.edu.cn; drk@ujs.edu.cn).

This article has supplementary material provided by the authors and color versions of one or more figures available at https://doi.org/10.1109/TPEL.2023.3268746.

Digital Object Identifier 10.1109/TPEL.2023.3268746

actual control process, especially in the communication network [16], which will adversely affect the control effect. Meanwhile, the vehicle response after mode switching will exhibit the characteristics of fluctuation and oscillation, and it cannot quickly converge to the ideal state, thus causing the switching instability [17].

Dong et al. [18] designed a six-stage coordinated controller, which consists of a feed-forward and feedback controller of the clutch and a torque compensation of the motor, and verified that the mode switching smoothness can be improved under the time-delay effect of the clutch actuator. Based on the different transmission delays of power source, liang et al. [19], [20] designed H_∞/H_2 coordinated controller with input constraints and H_∞ coordinated control law with state feedback. A coordinated control algorithm combining engine torque prediction and motor precompensation is proposed by Zeng et al. [21], which solved the problem that the motor torque compensation is not timely caused by the control delay of the subcontroller. In addition, a multimodule fusion time-delay-compensated coordinated control strategy for vehicle communication network is designed earlier by the author of this article to achieve steady convergence of engine speed and significant reduction of mode-switching jerk [22].

In fact, there are various structural parameter perturbations and external disturbances except the time delay factor in the dynamic process of PS-HEV. Chen et al. [23] clearly pointed out that the torque output disturbance of the engine and the driving condition disturbance of the vehicle will directly act on the vehicle, thereby causing obvious longitudinal jerk. Some scholars have conducted robustness research on the coordinated control strategies for different factors such as driving styles [24], vehicle load [25], torsion damping springs and equivalent damping coefficients of drive shafts [26].

However, the system time delay and disturbance are the coexisting factors in the actual control process of PS-HEV. No scholars have carried out related research on the mode switching control considering the coupling effect of the two factors so far, which inevitably reduces the controller effect in practical applications. Therefore, comprehensive consideration of the abovementioned factors in the mode switching process is a necessary factor that cannot be ignored in the study of the transient switching control, and it has important guiding significance for improving the practicability of the coordinated controller.

The innovations and main contributions are as follows: the control problem of multiple power sources caused by the simultaneous action of time delay and disturbance factors in the mode switching process of PS-HEV is creatively pointed out in this article, and the fact that their coupling could easily lead to system control performance degradation and even instability is deeply revealed. Then, the idea of a compound switching control system based on Markov [27] delay prediction and interference observation theory is innovatively proposed, and the accurate disturbance estimation of the extended state observer (ESO) with time delay factors for PS-HEV is realized for the first time. Compared with the traditional switching control, the introduction of delay prediction and ESO design incorporating time delay makes the control system more effective and stable, which is the biggest difference between the control method proposed in this article and the existing method.

The rest of this article is organized as follows. In Section II, the basic structure and the power split characteristics of the PS-HEV and the main problem caused are illustrated. In Section III, the unconventional ESO fused with Markov chain prediction models is constructed to accurately estimate the system interference under the influence of time delay, and the compound dynamic switching control incorporating multiple modules is presented afterwards. Then, the corresponding simulation and test results are conducted in Section IV. Finally, Section V concludes this article.

II. Power-Split System and Problem Description

A. Power-Split System Structure

The power-split system studied in this article is shown in Fig. 1. Wherein, the engine is connected to the planet carriers of the front planetary gear (PG), the motor MG1 is connected to the sun gear of the front PG, while the motor MG2 is connected to the sun gear of the rear PG. The ring gear of the rear PG is fixed. The front gear ring and the rear planet carrier are connected together to transmit and then output power. In particular, the decoupling of the engine speed and torque could be achieved by controlling MG1 and MG2. Meanwhile, the engine speed could be regulated by adjusting the torque of MG1, thereby changing the operating range of the engine and reducing the fuel consumption.

Let $i = \omega_E/\omega_{\text{out}}$ be the transmission ratio of the power-split mechanism, and $\lambda = k_1/(1+k_1)$ be the critical transmission ratio, then when $i = \lambda$, it belongs to the purely mechanical condition. When the coupling mechanism is in a balanced state, the rotational speed and torque of the motor MG1 are as follows (see Appendix 1):

$$\omega_{MG1} = k_1\left(\frac{1}{\lambda} - \frac{1}{i}\right)\omega_E \tag{1}$$

$$T_{MG1} = -\frac{1}{1+k_1}T_E = -\frac{\lambda}{k_1}T_E \tag{2}$$

Then, the speed and torque of the motor MG2 can be obtained

$$\omega_{MG2} = \frac{1+k_2}{i}\omega_E \tag{3}$$

$$T_{MG2} = \frac{i-\lambda}{1+k_2}\cdot\frac{\eta_{MG1}^{\delta_{MG1}}}{\eta_{MG2}^{\delta_{MG2}}}T_E. \tag{4}$$

The output speed and torque of the power-split coupling mechanism can be deduced subsequently

$$\omega_{out} = \frac{1}{i}\omega_E \tag{5}$$

$$T_{out} = \left(\lambda + (i-\lambda)\cdot\frac{\eta_{MG1}^{\delta_{MG1}}}{\eta_{MG2}^{\delta_{MG2}}}\right)T_E. \tag{6}$$

According to (1)–(6), as the transmission ratio i changes, the power flow direction in the coupling mechanism is also different. When i is greater than λ, as shown in Fig. 1(a), one part of the

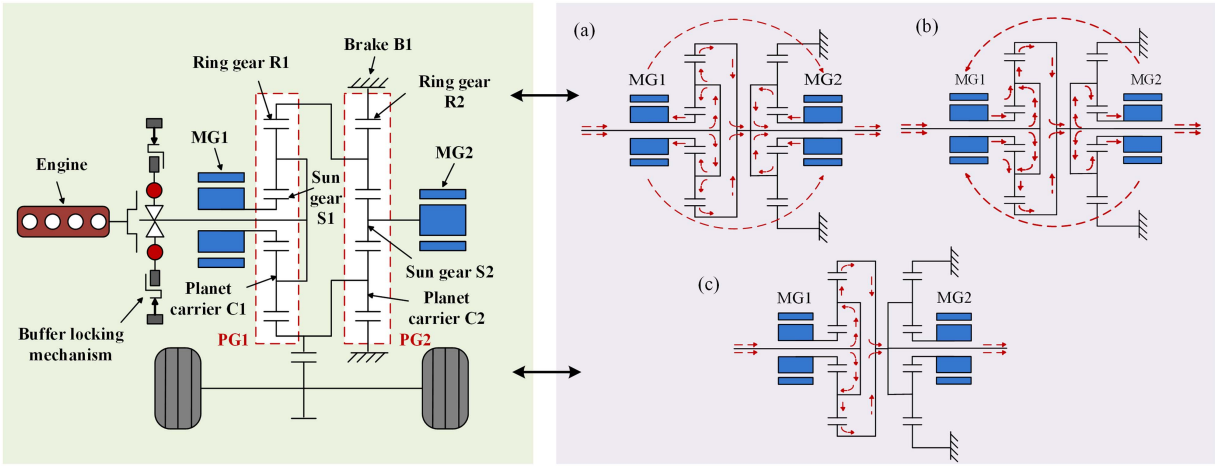

Fig. 1. Power coupling mechanism with dual planetary gears and its power flow characteristics. (a) MG1 works in power generation mode, while MG2 works in electric mode. (b) MG1 works in electric mode, while MG2 works in power generation mode. (c) Neither MG1 nor MG2 works.

engine power flows through the front row planetary components to drive the vehicle, and the other part is transmitted to the motor MG1 through the sun gear of the front planetary row, converted into electric power and stored in the battery pack. When i is relatively small, the engine power and the power of MG1 first converge at the ring gear of the front planetary row, and then split at the planetary carrier of the rear planetary row. Part of the mechanical power is converted into electric power by the motor MG2 subsequently, and the other part drives the vehicle through the output shaft [see Fig. 1(b)]. Once i is equal to λ, the engine power is transferred directly to the output shaft [see Fig. 1(c)].

Since the E-H switching process from the electric driving mode to the hybrid driving mode (E-H switching process) involves various intermediate states such as the starting and speed regulating process of the engine, it is more complicated than other switching process. Therefore, this article focuses on the dynamic characteristics of the system during the E-H switching process.

By analyzing the power split characteristics and transient dynamic behavior, the dynamic model of the power coupling mechanism (7), and the transient switching Simulink model of the vehicle are completed. A conventional basic motor torque compensation control (BMTCC) strategy is proposed to compensate for the torque lag characteristics of the engine and the reduction of the mode switching jerk is proved. For the specific derivation process, please refer to the literature [22], [23], which will not be repeated in this article. The key components of the whole vehicle are shown in Table S1 and Appendix 2 [22]

$$\begin{bmatrix} T_E + T_{MG1} + (1+k_2)T_{MG2} - T_{out} \\ T_E + (1+k_1)T_{MG1} \end{bmatrix} = \begin{bmatrix} I_{11} & I_{12} \\ I_{21} & I_{22} \end{bmatrix} \begin{bmatrix} \dot{\omega}_E \\ \dot{\omega}_{out} \end{bmatrix}. \tag{7}$$

B. Problem Description

In previous work, the author has explored the influence of different communication network time delay, engine torque disturbance d_1 and driving condition disturbance d_2 on motor compensation control, and proved the fact that time delay and disturbance have deteriorated the smoothness of mode switching, and raised corresponding improved control strategies ultimately [22], [23]. It is worth noting that in the actual driving process of the vehicle, time delay, and disturbance exist simultaneously [28], ignoring either one may deteriorate the control effect and robustness, thereby reducing the practicability of the controller.

Fig. 2 shows the influence of time delay and disturbances on the mode switching response of the vehicle system without any relevant control strategy. It can be obtained that regardless of time delay or disturbances, the basic motor compensation control strategy could still maintain the target vehicle speed tracking effect, correspondingly there is no significant difference among three cases [see Fig. 2(a) and (b)] but the other two power sources responded differently. Comparing the system response with only time delay and the system response with only disturbance, it can be found that the time delay is more significant for the system speed instability [see Fig. 2(c) and (f)], and the target vehicle speed tracking is more stable [see Fig. 2(d)], even the mode switching jerk caused is relatively small [see Fig. 2(e)]. Compared with the response with only time delay, when the time delay and disturbance exist at the same time, the speed oscillation amplitude of the power source is slightly larger, and the corresponding oscillation intensity of the mode switching jerk and vehicle speed tracking error are also greater than that of the response with only disturbance. In a word, the coexistence of system time delay and disturbance factors will aggravate the rotational speed instability of the power source, and greatly deteriorate the mode switching quality and the tracking stability of the vehicle target speed.

III. Dynamic Switching Control of PS-HEV Based on Time Delay Prediction and Interference Compensation

A. Design of ESO Incorporating Time Delay

If the controlled object is a first-order inertia-increased time-delay system, and the time delay is too large or the controlled object is sensitive to it, the accuracy of the conventional observer

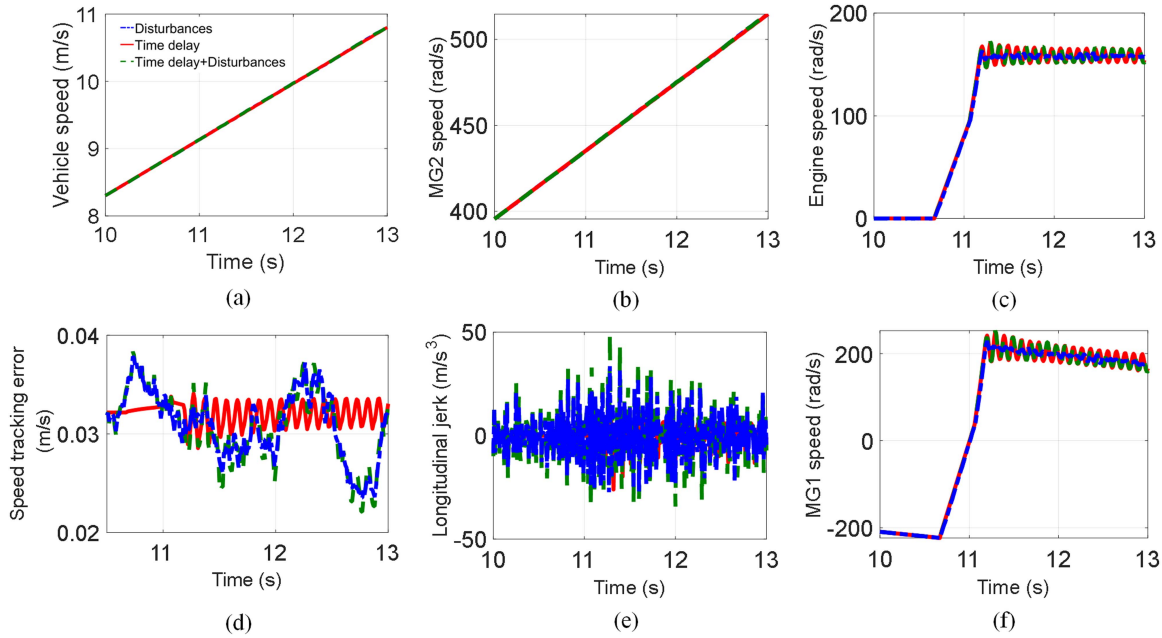

Fig. 2. Influence of time delay and disturbance on the mode switching response under basic motor compensation control strategy.

ignoring the time delay will be unsatisfactory, thus affecting the subsequent control effect [28].

Taking the improved second-order linear ESO previously designed by the author as an example [23], the influence of the time-varying communication delay in the forward channels of MG1 and MG2 on the interferences estimation of the observer is deeply studied in this article. Fig. S1 in Appendix 3 gives the comparison of observer interferences estimation in four cases shown in Table S2.

The results show that when the time delay at the MG1 terminal is ignored, the observer will fall into a situation in which the engine speed tracking error e_1 increases significantly, resulting in a worsening accuracy of d_1. Besides, the time delays of MG1 and MG2 both have an important influence on the output shaft torque disturbance estimation, and the more time delay factors are ignored, the greater the corresponding disturbance estimation error (see Appendix 3).

Therefore, under the premise of considering time delay and interference factors, an unconventional state observer [29] that integrates time delay factors must be designed to accurately estimate external interference, which also lays the foundation for subsequent interference suppression control.

Because of the importance of engine dynamic performance and road conditions for mode switching smoothness, the coupling mechanism model including the disturbances could be obtained

$$\begin{bmatrix}\dot{\omega}_E \\ \dot{\omega}_{\text{out}}\end{bmatrix} = B\cdot \begin{bmatrix} T_{\text{E}} + d_1 + T_{\text{MG1}} + (1+k_2)T_{\text{MG2}} - T_{\text{out}} - d_2 \\ T_{\text{E}} + d_1 + (1+k_1)T_{\text{MG1}} \end{bmatrix} \tag{8}$$

$$B = \begin{bmatrix} I_{11} & I_{12} \\ I_{21} & I_{22} \end{bmatrix}^{-1}. \tag{9}$$

Then, it could be transformed into the following state-space model:

$$\dot{y} = B \cdot U + d \tag{10}$$

$$y = \begin{bmatrix} \omega_E \\ \omega_{out} \end{bmatrix} \tag{11}$$

$$U = \begin{bmatrix} T_{\text{E}} + T_{\text{MG1}} + (1+k_2)T_{\text{MG2}} - T_{\text{out}} \\ T_{\text{E}} + (1+k_1)T_{\text{MG1}} \end{bmatrix} \tag{12}$$

$$d = B \cdot \begin{bmatrix} d_1 - d_2 \\ d_1 \end{bmatrix}. \tag{13}$$

According to the principle of the ESO, a new extended state vector is constructed

$$\bar{y} = d. \tag{14}$$

Combined with the Smith prediction idea, a predictive ESO, as shown in Fig. 3(a) is proposed, where *U(t)* is the power source torque command issued by the upper-layer coordinated controller at time *t*, *y(t-τ)* is the corresponding delayed output. The PS-HEV model refers to the vehicle dynamics model, and *y(t-* $\hat{\tau}$ *)* and $y_m(t)$ are the output of the model, respectively.

According to the Smith prediction theory, the prediction output without time delay could be obtained as follows:

$$y_p(t) = y(t-\tau) - y(t-\hat{\tau}) + y_m(t). \tag{15}$$

The system output without time delay is predicted by the approximate information of the PS-HEV model, and then the predicted output $y_p(t)$ is sent to the ESO, thereby realizing the synchronization of the observer information. The specific

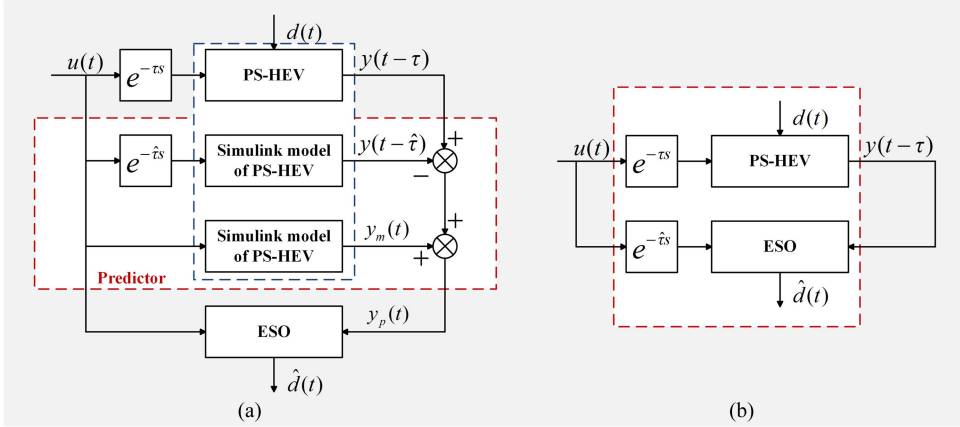

Fig. 3. Structure of ESO with time delay. (a) Predictive ESO. (b) ESO with delayed input.

formula for the predictive ESO can be derived

$$\begin{cases} e(t) = Z_1(t) - y_p(t) \\ \dot{Z}_1(t) = Z_2(t) + B \cdot U(t) - \beta_0 e(t) \\ \dot{Z}_2(t) = -\beta_1 \left[\dot{e}(t) + (\beta_0 + 1)e(t)\right] \end{cases} \tag{16}$$

where

$$\boldsymbol{\beta}_0 = \begin{bmatrix} \beta_{01} & 0 \\ 0 & \beta_{02} \end{bmatrix} \tag{17}$$

$$\boldsymbol{\beta}_1 = \begin{bmatrix} \beta_{11} & 0 \\ 0 & \beta_{12} \end{bmatrix}. \tag{18}$$

The observer parameters are tuned by multiobjective genetic algorithm, and the corresponding multiobjective optimization model is as follows:

$$\begin{cases} \min \varphi = f(x) = f(\varphi_1, \varphi_2) \\ \varphi_1 = \int_0^{t_f} \left[Z_1^T(t) R_p Z_1(t) - y_p^T(t) R_p y_p(t)\right] dt \\ \varphi_2 = \int_0^{t_f} \left[Z_2^T(t) Q_p Z_2(t) - \bar{y}^T(t) Q_p \bar{y}(t)\right] dt \\ x = (\beta_{01}, \beta_{02}, \beta_{11}, \beta_{12}) \in R^4 \\ \varphi = (\varphi_1, \varphi_2) \in R^2. \end{cases} \tag{19}$$

Although the predictive ESO could greatly improve the observation accuracy, it needs an approximate estimation of the time delay τ to obtain $\hat{\tau}$, and also requires a more accurate plant model. From the perspective of the system output y, the predictive ESO obtains the object output without time delay through the design of the predictor, and realizes the synchronization of the two inputs. Therefore, if the input U of the plant is delayed, the observer input can also be kept synchronized. Based on this, an ESO with delayed input is proposed.

A delay module between the control variable U and the observer is added in the ESO with delayed input, as shown in Fig. 3(b), so that U is synchronized with the output y, which is convenient for the observer to estimate the time-delay state of the system [30].

Thus, the ESO with delayed input could be obtained as follows:

$$\begin{cases} e(t) = Z_1(t) - y(t-\tau) \\ \dot{Z}_1(t) = Z_2(t) + B \cdot U(t-\hat{\tau}) - \beta_0 e(t) \\ \dot{Z}_2(t) = -\beta_1 \left[\dot{e}(t) + (\beta_0 + 1)e(t)\right]. \end{cases} \tag{20}$$

The multiobjective optimization model of the corresponding observer parameters is as follows:

$$\begin{cases} \min \varphi = f(x) = f(\varphi_1, \varphi_2) \\ \varphi_1 = \int_0^{t_f} \left[Z_1^T(t) R_l Z_1(t) - y^T(t-\tau) R_l y(t-\tau)\right] dt \\ \varphi_2 = \int_0^{t_f} \left[Z_2^T(t) Q_l Z_2(t) - \bar{y}^T(t) Q_l \bar{y}(t)\right] dt \\ x = (\beta_{01}, \beta_{02}, \beta_{11}, \beta_{12}) \in R^4 \\ \varphi = (\varphi_1, \varphi_2) \in R^2. \end{cases} \tag{21}$$

In addition, the stability analysis of ESO with delayed input is given as follows, which is similar to the stability derivation of the predictive ESO and will not be repeated.

If

$$\begin{aligned} X_1 &= e = Z_1 - y(t-\tau) \\ e_2 &= Z_2 - d. \end{aligned} \tag{22}$$

Then

$$\begin{aligned} \dot{X}_1 = \dot{e} &= X_2 = \dot{Z}_1 - \dot{y}(t-\tau) \\ &= Z_2 + B \cdot U(t-\hat{\tau}) - \beta_0 e - B \cdot U(t-\tau) - d \\ &\approx e_2 - \beta_0 e. \end{aligned} \tag{23}$$

In that way, the system equation of the observation error is

$$\begin{aligned} \dot{X}_1 &= X_2 \\ \dot{X}_2 = \dot{e}_2 - \beta_0 \dot{e} &= \dot{Z}_2 - \dot{d} - \beta_0 X_2 \\ &= -(\beta_1 + \beta_0) X_2 - w - \beta_1(\beta_0 + 1) X_1. \end{aligned} \tag{24}$$

The following quadratic function is designed:

$$W = -\beta_0 X_2^2. \tag{25}$$

From the Barbashin formula, the quadratic form V is attempted to be found

$$V = V_{11} X_1^2 + 2V_{12} X_1 X_2 + V_{22} X_2^2. \tag{26}$$

So that the derivative of (26) about the error system (24) satisfies the following equation:

$$\frac{dV}{dt} = 2W. \tag{27}$$

According to the error system (24) and Formula (26) and (27)

$$V=\frac{1}{\Delta}\left(\begin{vmatrix}0 & -\beta_1(\beta_0+1) & 0\\ 0 & -\beta_0-\beta_1 & -\beta_1(\beta_0+1)\\ -\beta_0 & 1 & -\beta_0-\beta_1\end{vmatrix}X_1^2 + 2\begin{vmatrix}0 & 0 & 0\\ 1 & 0 & -\beta_1(\beta_0+1)\\ 0 & -\beta_0 & -\beta_0-\beta_1\end{vmatrix}X_1X_2 + \begin{vmatrix}0 & -\beta_1(\beta_0+1) & 0\\ 1 & -\beta_0-\beta_1 & 0\\ 0 & 1 & -\beta_0\end{vmatrix}X_2^2\right). \tag{28}$$

The Lyapunov function of the error system is as follows:

$$V=\frac{1}{\Delta}\left[-\beta_0\beta_1^2(\beta_0+1)^2X_1^2-\beta_0\beta_1(\beta_0+1)X_2^2\right] \tag{29}$$

where

$$\Delta=\begin{vmatrix}0 & -\beta_1(\beta_0+1) & 0\\ 1 & -\beta_0-\beta_1 & -\beta_1((\beta_0+1))\\ 0 & 1 & -\beta_0-\beta_1\end{vmatrix}. \tag{30}$$

That is, the Lyapunov function is

$$V=\frac{\beta_0\beta_1(\beta_0+1)X_1^2+\beta_0X_2^2}{\beta_0+\beta_1}. \tag{31}$$

Then, its derivative is

$$\dot{V}=\frac{\partial V}{\partial X_1}\dot{X}_1+\frac{\partial V}{\partial X_2}\dot{X}_2 = -2\beta_0X_2^2-2\frac{\beta_0}{\beta_0+\beta_1}X_2w(t) \tag{32}$$

where

$$\dot{d}=w(t). \tag{33}$$

It can be obtained that V is positive definite and has infinite properties from the condition that β_0 and β_1 are positive values. When $w(t)=0$, the following conclusion could be summarized:

$$\dot{V}<0. \tag{34}$$

Therefore, the zero point of the error system is asymptotically stable over a wide range.

Comparing the abovementioned two ESO structures with time-delay fusion, it can be concluded that the ESO with delayed input has the following advantages.

1) Simple structure, less information required, and small computation.
2) High reachable bandwidth. The synchronization of the ESO with delayed input removes the time delay from the observation loop, rather than the main loop as in the predictive ESO, which improves the reachable bandwidth of the observer and its observation ability of disturbances [27].
3) The ESO with delayed input has slightly higher accuracy under the same observer parameters. Fig. 4 depicts the estimation error comparison of the abovementioned two ESO structures. The rms value of the ESO with delayed input is 1.216 Nm, which is slightly smaller than the predictive ESO [see Fig. 4(c)]. Similarly, the rms value of the ESO with delayed input is 0.16 Nm lower than the predictive ESO in terms of the output shaft torque disturbance estimation [see Fig. 4(d)], indicating that the ESO with delayed input is more effective in estimating two disturbances. Based on the abovementioned analysis, the ESO with delayed input is selected as the main tool for disturbance observation in this article.

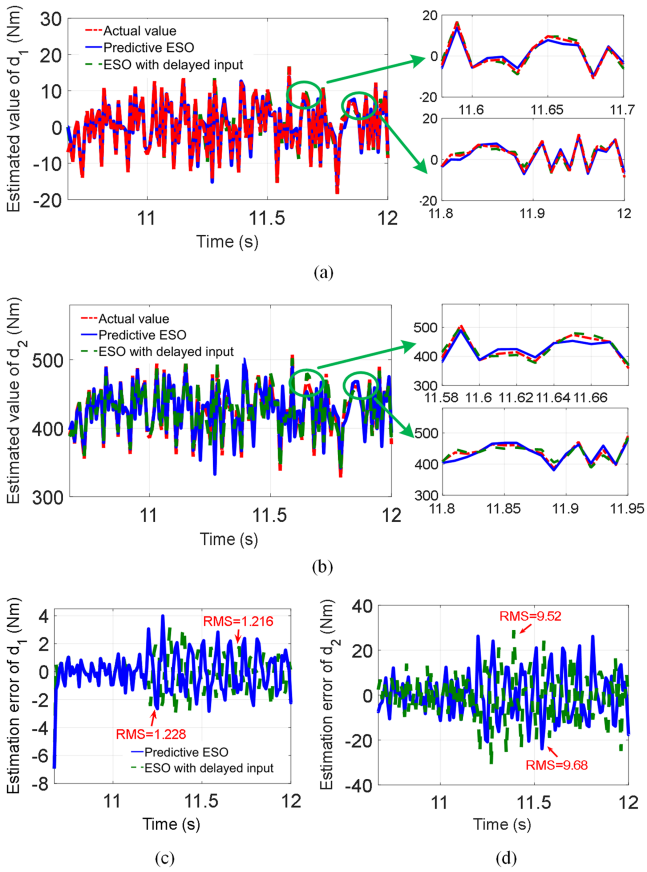

Fig. 4. Comparison of estimation accuracy of two extended state observers with time delay.

B. Construction of Markov Time Delay Prediction Module

Whether it is a predictive ESO or an ESO with delayed input, it is necessary to obtain an estimation of the time-varying communication delay τ in the forward channel of PS-HEV, which has an important impact on the observation accuracy of the observer [31]. Appendix 4 illustrates the fact that small or large estimation of the communication time delay at the MG1 terminal will cause obvious engine torque disturbance observation errors [see Fig. S2(a)], while the inaccurate estimation of the communication time delay at the MG1 and MG2 terminal both lead to significant errors on d_2 [Fig. S2(b), S3(b)]. In summary, the estimation accuracy of the communication time delay has a great influence on the observation accuracy of observer. The more precise the estimated value of the time delay, the more accurate the observation of the disturbances, and the higher the effectiveness of the subsequent disturbance compensation. Therefore, it

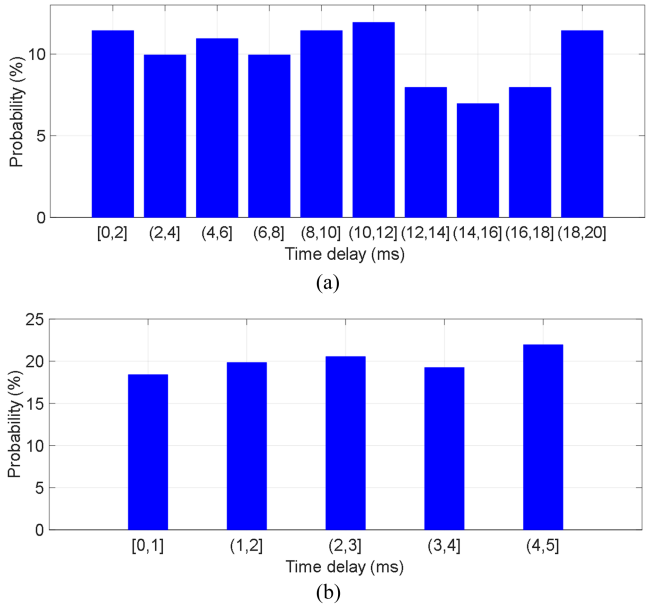

Fig. 5. Probability distribution of key delay factors. (a) Time delay distribution of MG1. (b) Time delay distribution of MG2.

is of great theoretical significance to explore methods that could accurately estimate or identify the system time delay.

Considering that the communication network delay at the current moment is usually related to the delay of the previous moment, but independent of the later time delay, it is completely in line with the no aftereffect of Markov theory, and the relevant proofs are detailed in Appendix 5. Based on the principle of Markov chain, the communication time delay of MG1 and MG2 is divided into 10 states and 5 states according to the interval of 2 ms and 1 ms, respectively, so that the time delay distribution after discretization can be obtained, as shown in Fig. 5. Fig. 6 describes the state transition probability diagrams of the abovementioned time delays. The time delay data at the next moment can be predicted according to the state transition probability, and its accuracy is also demonstrated in Table S5.

C. Dynamic Switching Control Strategy

In fact, model-based control methods and model-free control methods have been proposed successively since 1950 for the issue of time-delay control. Among them, model-based methods include Smith predictive compensation control, optimal control, and adaptive control. Model-free methods mainly refer to fuzzy Smith control and fuzzy PID control. The coordinated control problem of PS-HEV in the mode switching process belongs to the high-frequency transient control issue. For this process, the time-delay controller should have the characteristics of simple structure and small amount of calculation to obtain better control effects. The structure of Smith predictive controller is relatively simple, and it has been widely used in industrial process control and has strong practical value. By moving the time delay link outside the closed loop, the control quality of the system could be significantly improved. On the other hand, the compensation control could suppress the influence of the measurable disturbance on the output more quickly for the interference factors in the system. Aiming at the coexistence of time delay and interference factors in the mode switching process studied in this article, a compound switching control strategy shown in Fig. 7, which is composed of Smith time-delay predictive control and disturbance compensation control, could improve the anti-interference ability and control accuracy according to the automatic control theory. The compound switching control strategy in the controller derives the torque redistribution amount according to the corresponding prediction and compensation algorithm, and then the final torque commands [as shown in (35)–(42)] are transmitted to the underlying power source actuators through the in-vehicle communication network to control the operation of each component and the driving of the PS-HEV.

According to the control strategy, the torque distribution formula of the entire E-H mode switching process is deduced further. When the PS-HEV works in the pure electric mode driven by the motor MG2 alone, the torque of the engine is 0, and the motor MG1 controls the engine at the zero speed point. At present, the power of MG1 is transmitted to the engine through the front planetary carrier, while the power of MG2 is output to the wheels via the rear planetary carrier. Considering the influence of d_2, it is equivalently converted into the driving resistance torque, and estimated online by the observer, so as to realize the disturbance cancellation. The torque distribution of the two motors in pure electric mode is as follows by combining the steady-state lever model:

$$T_{MG1} = k_{p1}(\omega_E - 0) + k_{i1}\int(\omega_E - 0)dt \tag{35}$$

$$T_{MG2} = \frac{1}{1+k_2}T_{req} - \frac{1}{1+k_2}\hat{d}_2. \tag{36}$$

When the vehicle speed exceeds a certain threshold V_{thr} (this article is set to 32 km/h), the pure electric mode cannot meet the driving demand. It is necessary to start the engine to the idle speed $\omega_{E\text{-target}}$ (900 r/min) within 0.5 s, and the whole vehicle enters the engine cranking mode. In order to eliminate the impact of engine towing, the compensation torque ΔT_{MG2} is designed, and the observers are used to estimate the disturbances d_1 and d_2 to reduce the deterioration of the mode switching smoothness caused by the two disturbances. The target torques of motors MG1 and MG2 are as follows at this time:

$$T_{MG1} = -\frac{1}{1+k_1}T_{ef} + \frac{I_{11}}{1+k_1}\dot{\omega}_{E-target} - \frac{1}{1+k_1}\hat{d}_1 \tag{37}$$

$$T_{MG2} = \frac{1}{1+k_2}T_{req} - \frac{k_1}{(1+k_1)(1+k_2)}T_{ef} + \Delta T_{MG2} - \frac{1}{1+k_2}\hat{d}_2 - \frac{k_1}{(1+k_1)(1+k_2)}\hat{d}_1 \tag{38}$$

$$\Delta T_{MG2} = \left(\frac{I_{21}}{1+k_2} - \frac{I_{11}}{(1+k_1)(1+k_2)}\right)\dot{\omega}_E. \tag{39}$$

Once the engine speed exceeds the idle speed, the PS-HEV quickly switches to the hybrid driving mode. Then, the engine

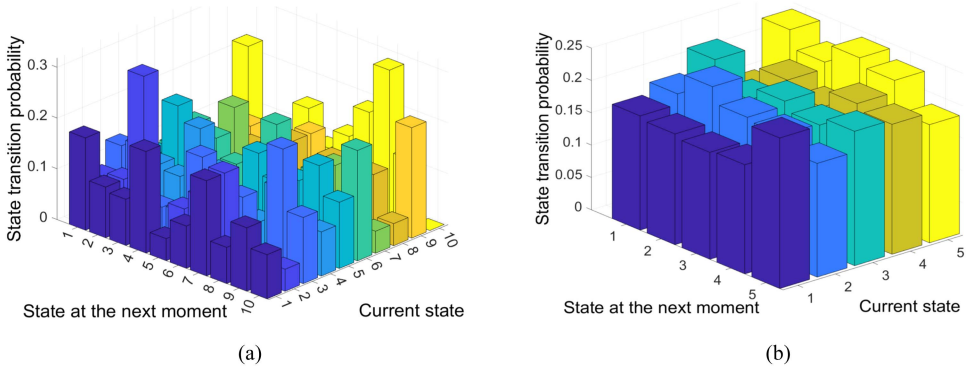

Fig. 6. Histogram of state transition probability of key time delay factors. (a) MG1. (b) MG2.

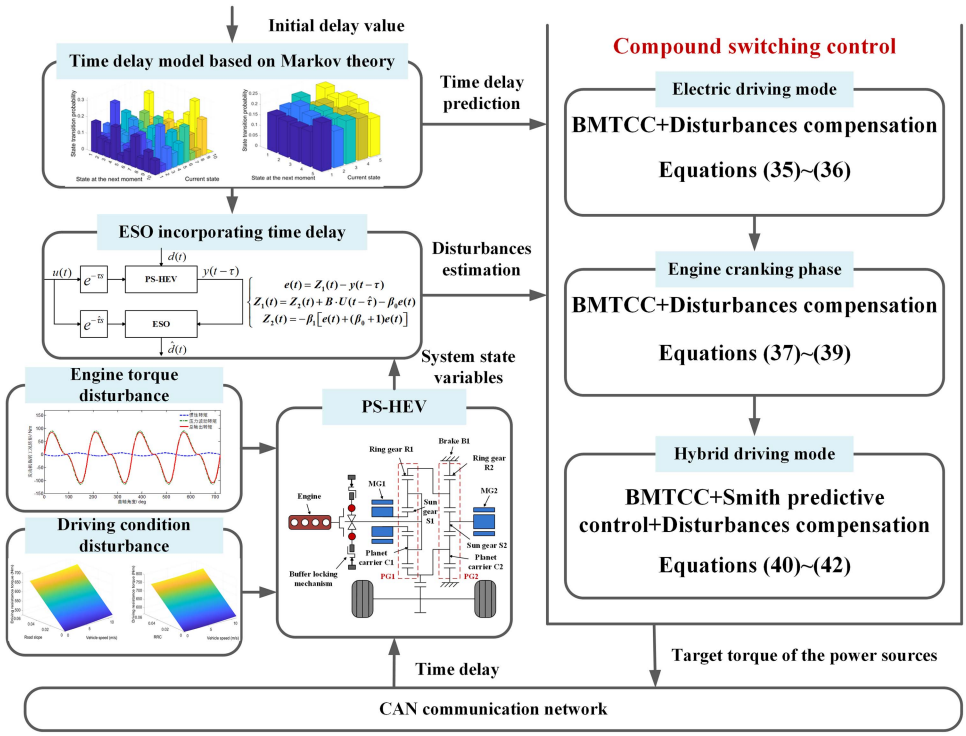

Fig. 7. Compound switching control block diagram.

outputs torque, and cooperates with the motor MG2 to drive the whole vehicle. The motor MG1 regulates the engine to work at the economical speed $\omega_{E\text{-}e}$ (1500 r/min). Based on the BMTCC, the Smith predictive controller (ΔT_{MG1}) is used to eliminate the system instability caused by the communication delay of the MG1, and the interference compensation is used to offset the jerk caused by two kinds of interferences

$$T_{MG1} = -\frac{1}{1+k_1}T_{E-est} + \frac{I_{11}}{1+k_1}\dot{\omega}_E + \Delta T_{MG1} - \frac{1}{1+k_1}\hat{d}_1 \tag{40}$$

$$\Delta T_{MG1} = k_p(\omega_{E-e} - \omega_E - e_{w-engine}) + k_i \int (\omega_{E-e} - \omega_E - e_{w-engine})dt \tag{41}$$

$$T_{MG2} = \frac{1}{1+k_2}T_{req} - \frac{k_1}{(1+k_1)(1+k_2)}T_{E-est} + \Delta T_{MG2} - \frac{1}{1+k_2}\hat{d}_2 - \frac{k_1}{(1+k_1)(1+k_2)}\hat{d}_1. \tag{42}$$

The parameters k_p and k_i in the Smith predictor are optimized by the particle swarm algorithm. The search area is a two-dimensional space, the population size is 100, and the nth particle can be expressed as

$$X_n = (x_{n1}, x_{n2})^T. \tag{43}$$

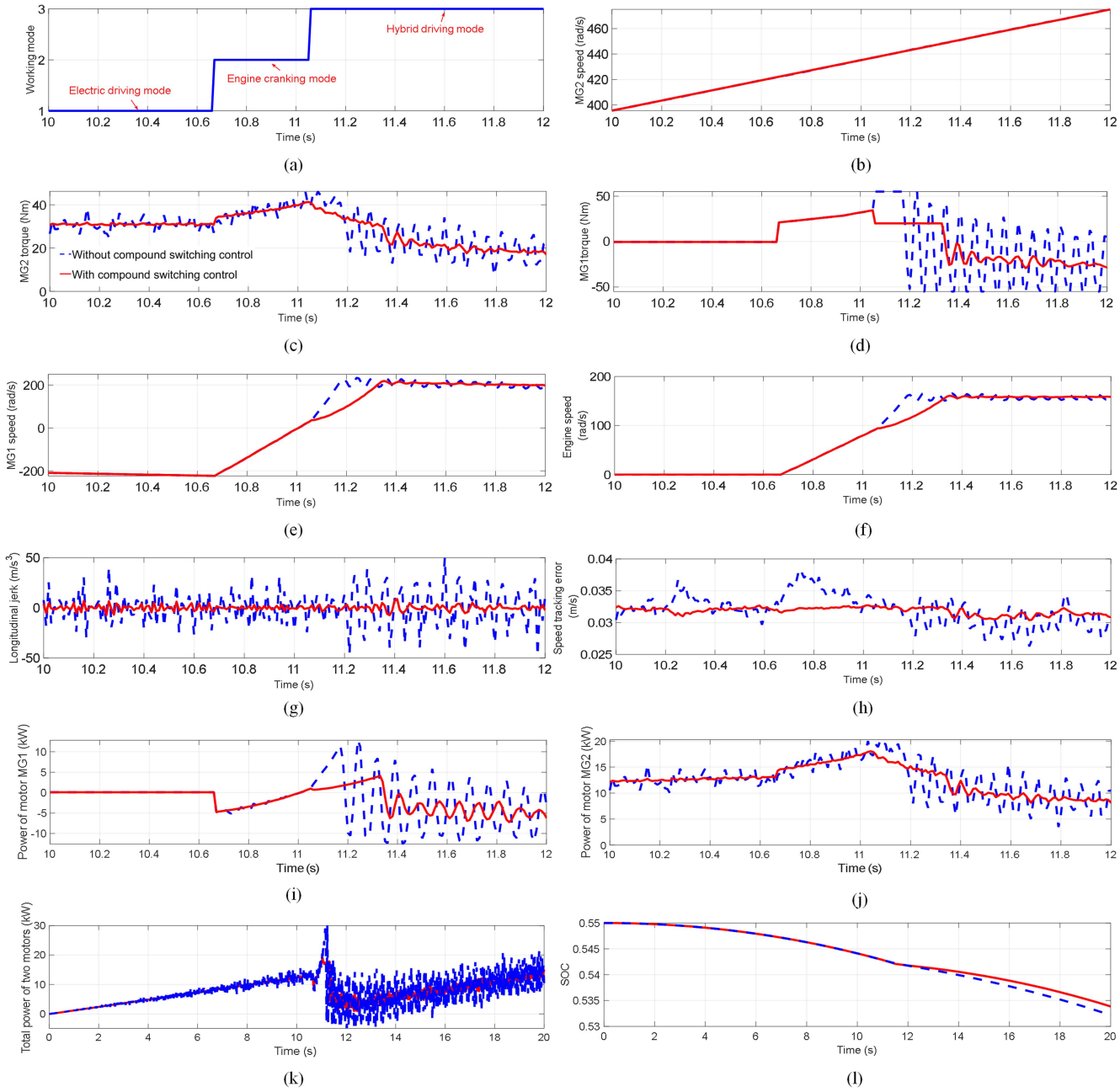

Fig. 8. Compound switching control effect.

The corresponding particle velocity, individual extremum, and group extremum are as follows:

$$V_n = (V_{n1}, V_{n2})^T \tag{44}$$

$$P_n = (P_{n1}, P_{n2})^T \tag{45}$$

$$P_g = (P_{g1}, P_{g2})^T. \tag{46}$$

Particle velocities and positions are updated according to (47) and (48)

$$V_n^{k+1} = \phi(k) V_n^k + \mu_1 r_1 \left(P_n^k - X_n^k\right) + \mu_2 r_2 \left(P_g^k - X_n^k\right) \tag{47}$$

$$X_n^{k+1} = X_n^k + V_n^{k+1} \tag{48}$$

where

$$\phi(k) = \phi_{start} - (\phi_{start} - \phi_{end}) \cdot \sin\left(\pi \left(\frac{k}{t_{k-\max}}\right)^2\right) \tag{49}$$

$$\mu_1 = \mu_{\max} - \sin\left(\frac{k\pi}{t_{k-\max}}\right) \tag{50}$$

$$\mu_2 = \mu_{\min} + \sin\left(\frac{k\pi}{t_{k-\max}}\right). \tag{51}$$

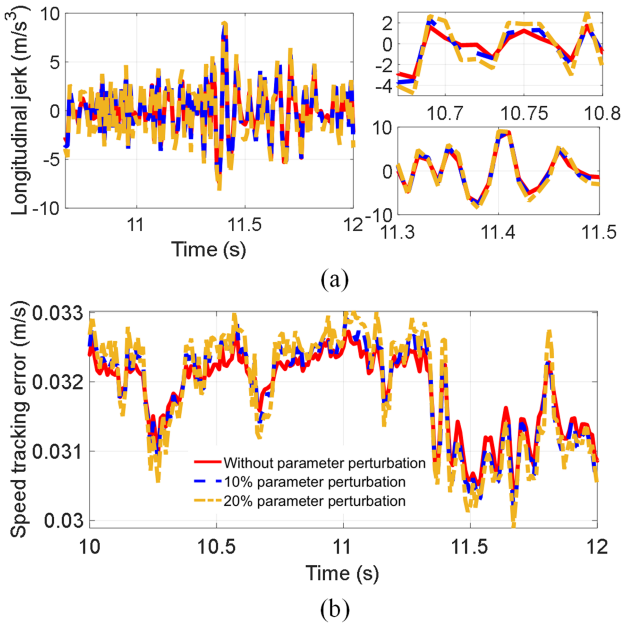

Fig. 9. Compound switching control effect under structural parameter perturbation of PS-HEV.

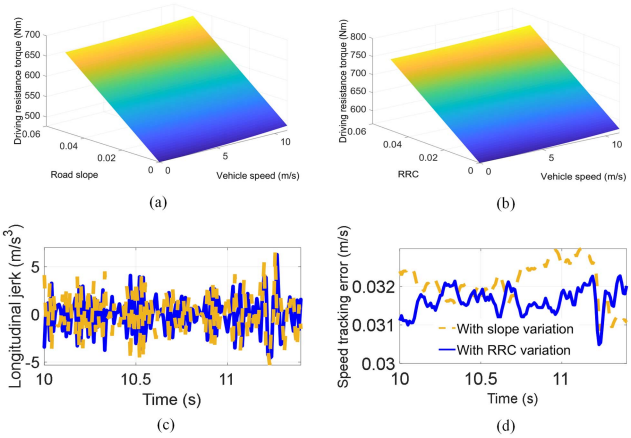

Fig. 10. Compound switching control effect under variable road conditions of PS-HEV.

The fitness function adopts the following error integration criterion:

$$P = \int_0^{\infty} t\left[e_j^T(t)e_j(t)\right]dt \tag{52}$$

where

$$e_j = \begin{bmatrix} \omega_E - \omega_{E-e} \\ j \end{bmatrix}. \tag{53}$$

The fitness of the updated particles is calculated through iteration, thereby updating the individual extremum and the group extremum. The iteration ends until the optimal solution of the parameters of the Smith predictor that satisfies the conditions is obtained.

IV. Simulation Analysis and HIL Test

Based on the model of the abovementioned compound switching control strategy, the performance simulation analysis is carried out on the MATLAB/Simulink software platform in this section. The observation gain matrices in ESO with delayed input are $\beta_0 = \text{diag}\{50\ 100\}$, $\beta_1 = \text{diag}\{125\ 130\}$. The final optimization results of parameters in the Smith predictor are $k_p = 0.5$, and $k_i = 0.0001$. The response results of PS-HEV are shown in Fig. 8.

It should be noted that the system response without compound switching control in this figure only refers to the result of the BMTCC[22]. It can be seen from Fig. 8(a) that the vehicle has been working in pure electric mode until 10.67 s. During this period, only the motor MG2 outputs torque to drive the vehicle, the motor MG1 is idling in the reverse direction [see Fig. 8(e)], and the engine is turned OFF [see Fig. 8(f)]. Due to the load torque interference caused by the driving conditions, the torque output of MG2 also showed a trend of fluctuation and oscillation successively [as shown by the dotted line in Fig. 8(c)], which causes a dramatic positive and negative jerk, up to 40.2 m/s^3 and 29.5 m/s^3, respectively, and even the maximum speed tracking error of 0.036 m/s [see Fig. 8(h)].

When the vehicle speed reaches 32 km/h at 10.67 s, it enters the engine cranking phase, and the ignition speed 900 r/min is reached at 11.07 s. Because of the fluctuation of engine drag resistance torque and load torque, the longitudinal jerk of the vehicle is up to 32.9 m/s^3, and the speed tracking error is as high as 0.038 m/s. After the engine is injected and ignited, the PS-HEV enters the hybrid driving mode, and MG1 maintains the engine speed to work at the economical speed. However, due to the simultaneous effect of time delay factors and disturbances, the system obviously presents the phenomenon of rotational speed instability [as shown in Fig. 8(e) and (f)], and the vehicle switching jerk increases significantly, which seriously affects the transition smoothness. It is worth noting that after adopting the compound switching control strategy, the torque, and power output curves of MG1 and MG2 are smoother through the interference compensation in the mode transition stages [as shown in Fig. 8(c), (d), (i), and (j)], the corresponding torque change rates and power consumption are smaller [see Fig. 8(k)], which results in higher SOC of battery [see Fig. 8(l)], more stable speed tracking effect, and even less longitudinal jerk within the range of [−10 m/s^3, 10 m/s^3]. Since the torque variation of MG1 is limited in the compound switching control, the time for the engine to reach the steady-state economical speed is slightly longer, which is within an acceptable range.

Furthermore, in order to test the robustness and road adaptability of the compound switching control strategy, a series of simulation studies on the relevant parameter perturbations are carried out. Fig. 9 compares the control effects under different perturbations of PS-HEV structural parameters (full load mass, moment of inertia). The results show that the higher the degree of perturbation of the abovementioned parameters, the greater the switching jerk and the speed tracking error, but the increase is relatively small, which indicates that the compound switching control strategy could still effectively maintain the switching smoothness and speed tracking stability.

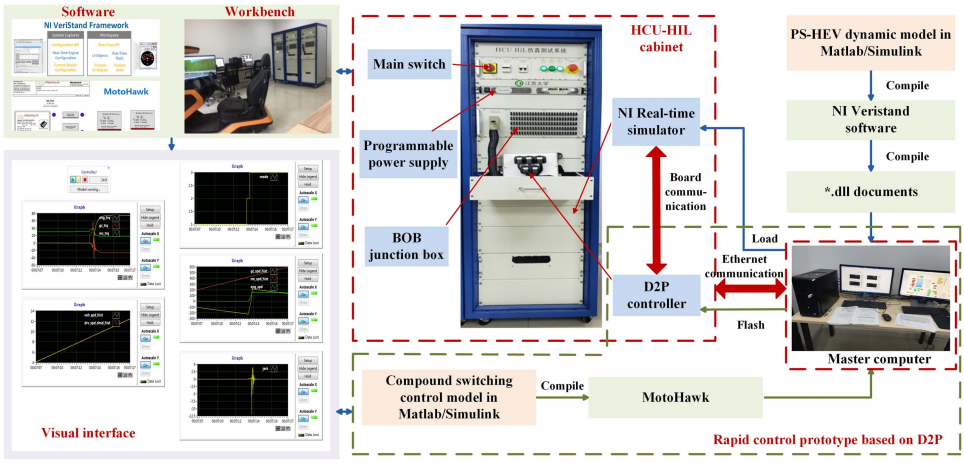

Fig. 11. HIL test plan for switching control strategy.

Fig. 10(a) and (b) show the curves of the vehicle resistance torque with the change of road slope, rolling resistance coefficient (RRC) and vehicle speed, and Fig. 10(c) and (d) plot the variation of the control effect under different driving conditions. It can be concluded that the whole vehicle driving resistance torque has a positive correlation with road slope, RRC and vehicle speed, and the compound control also exhibits a good adaptability to the abovementioned changes. Since the change of road slope per unit interval could cause greater change of driving resistance torque, its switching jerk and speed tracking error are slightly larger.

To further verify the correctness of the simulation, a hardware-in-the-loop (HIL) test was carried out subsequently. The HIL test scheme of the coordinated control strategy, as shown in Fig. 11 is proposed. The hardware platforms of HIL experiment for PS-HEV coordinated control strategy verification mainly include the test cabinet and development to production (D2P) controller. The test cabinet is mainly composed of power management module, programmable power supply, NI real-time simulator, signal conditioning box, load simulation box, BOB junction box, and other components. The software platform is NI VeriStand specially developed for HIL simulation test by National Instruments, which could realize various functions such as hardware configuration management, hardware I/O interface configuration and mapping, simulation model import, user interface creation, data recording and playback, fault signal simulation, and report generation. The rapid control prototyping platform used for switching controller development is D2P system, which mainly includes MotoHawk, a modeling software based on MATLAB/Simulink, MotoTune for program flashing and data calibration, and other controller hardware.

The basic principle of the HIL test scheme is as follows.

1) Dividing the built simulation model into the controller part and the controlled object part, and then the controlled object model can be transcoded into a $*$.dll file and loaded into the NI real-time simulator by using the NI Veristand software in the host computer. Meanwhile, the controller model is compiled and flashed to the D2P controller through MotoHawk.
2) Running the HCU-HIL test cabinet, the NI real-time simulation will send the current vehicle speed, target torque, engine speed, motor speed, output shaft speed, and other information in the controlled object model to the D2P controller through the board. The D2P controller calculates and processes the collected data signals, and outputs the processed signals and control commands to the controlled model in the NI real-time simulator through the board card.
3) The controlled model responds after receiving the control commands, and the corresponding output signal of the object is collected and transmitted to the controller again, thus forming a closed-loop test. Through the visual interface, the user could observe and record the key response parameter curve of the vehicle, which is helpful to analyze the current state information of the vehicle.

Fig. 12 gives the comparison results of this experiment and simulation. It can be seen from Fig. 12 that when there are time delay and external interferences in the whole E-H mode switching process, the ESO with delayed input could accurately estimate the key disturbances, thus, the compound coordinated control strategy in the HIL test could effectively distribute the torque of the power sources and stabilize the engine speed, so as to control the jerk in the ideal range, and the target vehicle speed tracking is relatively stable.

Although the system response trend in the HIL test is roughly consistent with the simulation result, there is inevitably some deviation. For example, the absolute value of the longitudinal jerk in the HIL test is slightly higher than the simulation result in most cases, and the vibration fluctuation intensity of the vehicle speed tracking is also significantly greater than the simulation result. The main reason for the deviation is that there is a certain system delay in signal I/O conversion, controller transcoding, and system hardware in the cabinet during HIL test operation, which causes controller time delay. At the same time, due to board communication and other factors, the state observer has a little deviation in the estimation of key interference. As a result,

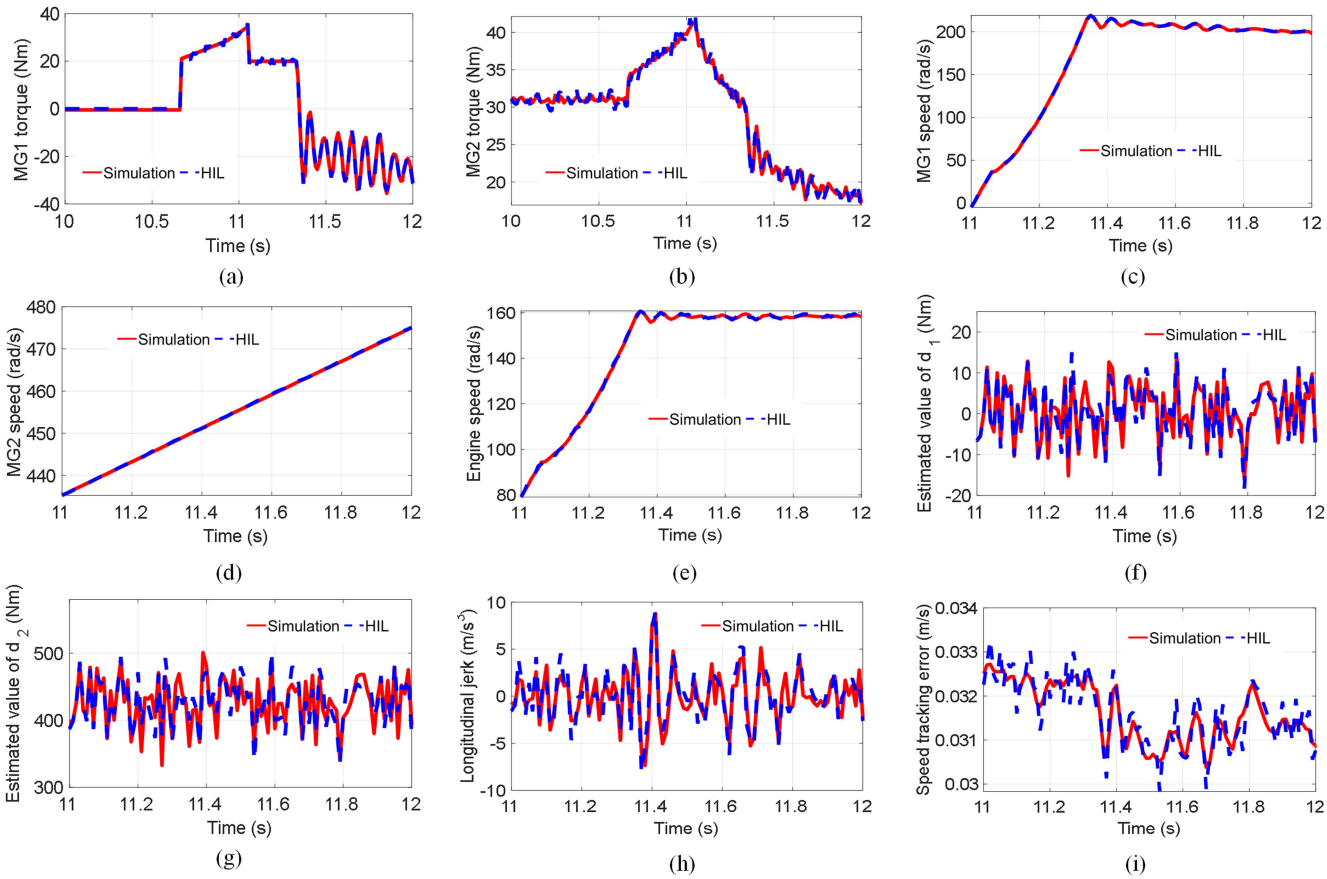

Fig. 12. Comparison between simulation and HIL of compound coordinated control strategy.

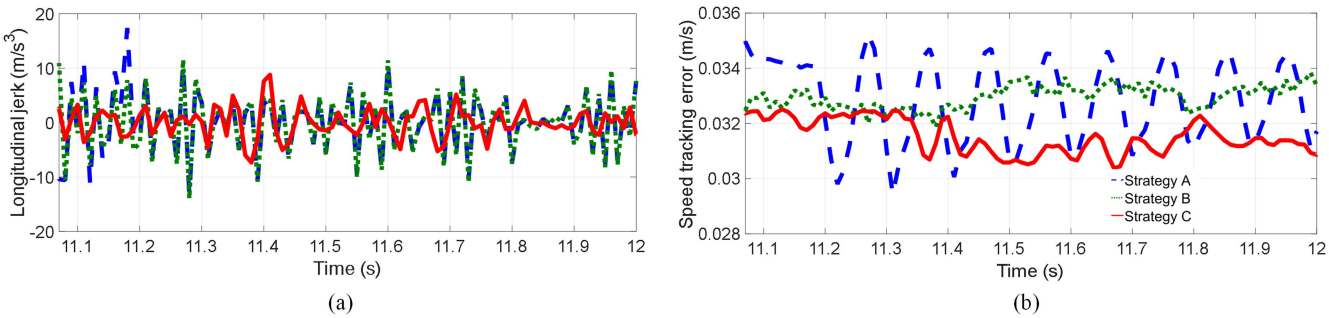

Fig. 13. Comparative HIL tests of three control strategies.

the controller parameters used in HIL test and MATLAB simulation are different, which makes the vehicle mode switching response not completely consistent in the two test environments.

Furthermore, three sets of comparative tests of different control strategies are conducted and the main results regarding the mode switching quality are shown in Fig. 13 and Table I. It is worth noting that under the same conditions of system disturbances, the mode switching jerk using the compound switching control strategy based on ESO with delayed input (Strategy C) in the HIL test only reaches a maximum of 9.18 m/s^3, which is significantly lower than that of the PS-HEV under the disturbance compensation control (strategy A). The reason is that the time delay compensation module in the compound control strategy makes the D2P controller adjust the controller parameters by default to deal with the deterioration of the control effect caused by the time delay, and the addition of the time-delay observer improves the accuracy of the disturbance estimation, which leads to a smaller jerk in the HIL test and smoother speed tracking as well. In addition, the comparison between strategy A and strategy B also shows the effectiveness of the Smith time-delay control module, which could significantly reduce the jerk of nearly 5 m/s^3 and the speed tracking error of 0.001 m/s.

In summary, all of these indicate the excellent switching smoothness, anti-interference and vehicle speed tracking stability of this strategy, and it also lays a theoretical foundation

TABLE I
COMPARISON RESULTS

	Control strategy type		Observer type	Longitudinal jerk (m/s^3)		Vehicle speed tracking error (m/s)	
				Peak value	RMS	Peak value	RMS
Simulation	Strategy A	Only disturbance compensation control	Traditional ESO	18.94	3.49	0.0346	0.0334
	Strategy B	Compound switching control	Traditional ESO	13.48	2.85	0.0335	0.0326
	Strategy C	Compound switching control	ESO with delayed input	9.07	1.45	0.0327	0.0322
HIL test	Strategy A	Only disturbance compensation control	Traditional ESO	19.24	3.62	0.0349	0.0336
	Strategy B	Compound switching control	Traditional ESO	14.53	2.97	0.0338	0.0331
	Strategy C	Compound switching control	ESO with delayed input	9.18	1.63	0.0334	0.0327

and technical support for the optimal design of the coordination controller of PS-HEV.

V. CONCLUSION

This article innovatively proposes the compound switching control strategy based on time delay prediction and interference compensation of PS-HEV, and the comprehensive performance is effectively improved. The main conclusions are as follows.

1) This article reveals the fact that the coexistence of system time delay and interference factors will aggravate the speed instability of the power source, greatly deteriorate the mode switching quality.
2) Two ESO structures with time-delay fusion are designed, and the ESO with delayed input is selected as the main tool for disturbance observation in terms of practicality, reachable bandwidth, and observation accuracy.
3) A one-step Markov chain time-delay prediction model is built, and a compound switching control strategy combining multimodule fusion of time delay prediction, observer, predictive control, and interference compensation is proposed, which effectively maintains the mode switching stability and smoothness.
4) The verification test of the switching controller is only carried out based on the hardware-in-the-loop platform in this article, which is inevitably different from the actual test conditions and environment. Combining the prototype bench and real vehicle, the detection, calibration, and optimization of the controller performance will be the focus of follow-up research.

REFERENCES

[1] S. Hemmati, N. Doshi, D. Hanover, C. Morgan, and M. Shahbakhti, "Integrated cabin heating and powertrain thermal energy management for a connected hybrid electric vehicle," *Appl. Energy*, vol. 283, pp. 1–22, Feb. 2021.

[2] S. Zhou, Z. Chen, D. Huang, and T. Lin, "Model prediction and rule based energy management strategy for a plug-in hybrid electric vehicle with hybrid energy storage system," *IEEE Trans. Power Electron.*, vol. 36, no. 5, pp. 5926–5940, May 2021.

[3] Y. Zhang, R. Ma, D. Zhao, Y. Huangfu, and W. Liu, "A novel energy management strategy based on dual reward function Q-learning for fuel cell hybrid electric vehicle," *IEEE Trans. Ind. Electron.*, vol. 69, no. 2, pp. 1537–1547, Feb. 2022.

[4] W. Wang et al., "A multi-objective optimization energy management strategy for power split HEV based on velocity prediction," *Energy*, vol. 238, pp. 1–14, Jan. 2022.

[5] K. C. Bayindir, M. A. Gozukucuk, and A. Teke, "A comprehensive overview of hybrid electric vehicle: Powertrain configurations, powertrain control techniques and electronic control units," *Energy Convers. Manage.*, vol. 52, no. 2, pp. 1305–1313, Feb. 2011.

[6] T. Deng, P. Tang, Z. Su, and Y. Luo, "Systematic design and optimization method of multimode hybrid electric vehicles based on equivalent tree graph," *IEEE Trans. Power Electron.*, vol. 35, no. 12, pp. 13465–13474, Dec. 2020.

[7] Y. Su, M. Hu, J. Huang, D. Qin, C. Fu, and Y. Zhang, "Dynamic torque coordinated control considering engine starting conditions for a power-split plug-in hybrid electric vehicle," *Appl. Sci.*, vol. 11, no. 5, pp. 1–26, Mar. 2021.

[8] Y. Tong, *Study on the Coordinated Control Issue in Parallel Hybrid Electric System*. Beijing, China: Tsinghua Univ., 2004.

[9] Y. Lin, D. Qin, Y. Liu, and Y. Yang, "Control strategy for all the mode-switches of hybrid electric vehicle," *Adv. Mech. Eng.*, vol. 8, no. 11, pp. 1–17, Nov. 2016.

[10] K. Huang, C. Xiang, Y. Ma, W. Wang, and R. Langari, "Mode shift control for a hybrid heavy-duty vehicle with power-split transmission," *Energies*, vol. 10, no. 2, pp. 1–18, Feb. 2017.

[11] M. Razi, N. Murgovski, T. Mckelvey, and T. Wilk, "Design and comparative analyses of optimal feedback controllers for hybrid electric vehicles," *IEEE Trans. Veh. Technol.*, vol. 70, no. 4, pp. 2979–2993, Apr. 2021.

[12] Z. Zhao, X. Tang, J. Fu, and J. Fan, "Optimal control of engine shutdown for power-split hybrid system," *Automobile Eng.*, vol. 42, no. 8, pp. 993–999, Aug. 2020.

[13] F. Zhu, L. Chen, C. Yin, and J. Shu, "Dynamic modelling and systematic control during the mode transition for a multi-mode hybrid electric vehicle," *Proc. Inst. Mech. Engineers, D, J. Automobile Eng.*, vol. 227, no. 7, pp. 1007–1023, Jul. 2013.

[14] J. Chen and H. Hwang, "Engine automatic start–stop dynamic analysis and vibration reduction for a two-mode hybrid vehicle," *Proc. Inst. Mech. Engineers, D, J. Automobile Eng.*, vol. 227, no. 9, pp. 1303–1312, Sep. 2013.

[15] L. Du, Y. Guo, H. Zhan, and X. Duan, "Research on key technologies of multi-smart-agents based partially distributed control system for aero engine," *Int. Federation Autom. Control-Papers Online*, vol. 54, no. 10, pp. 483–487, Nov. 2021.

[16] M. Mehdi, C.-H. Kim, and M. Saad, "Robust centralized control for DC islanded microgrid considering communication network delay," *IEEE Access*, vol. 8, pp. 77765–77778, 2020.

[17] G. Song and C. Xu, "Stochastic optimal preview control of active vehicle suspension with time-delay consideration," *Trans. Chin. Soc. Agricultural Machinery*, vol. 44, no. 6, pp. 1–7, Jun. 2013.

[18] P. Dong, S. Wu, W. Guo, and X. Xu, "Coordinated clutch slip control for the engine start of vehicles with P2-hybrid automatic transmissions," *Mech. Mach. Theory*, vol. 153, no. 3, pp. 1–15, Nov. 2020.
[19] C. Liang, X. Xu, F. Wang, S. Wang, and Z. Zhou, "CAN-induced asynchronous random delays-considered mode transition system for DM-PHEV based on constrained output feedback robust control strategy," *IEEE Trans. Veh. Technol.*, vol. 71, no. 6, pp. 5995–6006, Jun. 2022.
[20] C. Liang, X. Xu, F. Wang, and Z. Zhou, "H-infinity non-clutch coordinated control for mode transition system of DM-PHEV with CAN-induced delays," *Nonlinear Dyn.*, vol. 107, pp. 1003–1021, Nov. 2021.
[21] X. Zeng et al., "A study on coordinated control of urban hybrid electric SUV based on dynamic characteristics of components," *Automot. Eng.*, vol. 40, no. 11, pp. 1255–1260, Nov. 2018.
[22] J. Wang, Y. Cai, L. Chen, D. Shi, S. Wang, and Z. Zhu, "Research on compound coordinated control for a power-split hybrid electric vehicle based on compensation of non-ideal communication network," *IEEE Trans. Veh. Technol.*, vol. 69, no. 12, pp. 14818–14833, Dec. 2020.
[23] L. Chen, J. Wang, Y. Cai, D. Shi, and R. Wang, "Mode transition control of a power-split hybrid electric vehicle based on improved extended state observer," *IEEE Access*, vol. 8, pp. 207260–207274, 2020.
[24] J. Sun, G. Xing, X. Liu, X. Fu, and C. Zhang, "A novel torque coordination control strategy of a single-shaft parallel hybrid electric vehicle based on model predictive control," *Math. Problems Eng.*, vol. 2015, pp. 1–12, Sep. 2015.
[25] J. Ding and X. Jiao, "A novel control method of clutch during mode transition of single-shaft parallel hybrid electric vehicles," *Electronics*, vol. 9, no. 1, pp. 1–16, Dec. 2019.
[26] Y. Su, M. Hu, L. Su, D. Qin, T. Zhang, and C. Fu, "Dynamic coordinated control during mode transition process for a compound power-split hybrid electric vehicle," *Mech. Syst. Signal Process.*, vol. 107, pp. 221–240, Jul. 2018.
[27] M. Vasilyeva, A. Tyrylgin, D. L. Brown, and A. Mondal, "Preconditioning Markov chain Monte Carlo method for geomechanical subsidence using multiscale method and machine learning technique," *J. Comput. Appl. Math.*, vol. 392, no. 5, pp. 1–29, Feb. 2021.
[28] W. Deng *Consensus of Multi-Agent System With Communication Delays and External Disturbances*. Harbin, China: Harbin Univ., 2020.
[29] Q. Zheng and Z. Gao, "Predictive active disturbance rejection control for processes with time delay," *Instrum. Soc. Amer. Trans.*, vol. 53, no. 4, pp. 873–881, Jul. 2014.
[30] S. Zhao and Z. Gao, "Modified active disturbance rejection control for time-delay systems," *Instrum. Soc. Amer. Trans.*, vol. 53, no. 4, pp. 882–888, Jul. 2014.
[31] W. Yu *Design and Stability Region Analysis of Active Disturbance Rejection Control for Time-Delay Systems*. Beijing, China: Beijing Univ., 2017.

Jiajia Wang was born in Xinyang, China, in 1992. She received the M.S. and Ph.D. degrees in vehicle engineering from Jiangsu University, Zhenjiang, China, in 2017 and 2021, respectively.

In 2021, she was with the School of Mechanical Engineering, Yangzhou University, Yangzhou, China. Her research interests include vehicle dynamic performance simulation and control, and hybrid electric vehicles.

Ruochen Wang was born in Henan province, China, in 1977. He received the B.S. and Ph.D. degrees in vehicle engineering from Jiangsu University, Jiangsu, China, in 2001 and 2006, respectively.

Mr. Wang is currently the Ph.D. supervisor and Associate Dean with the School of Automotive Engineering, Jiangsu University. He has authored and coauthored more than 120 academic papers, which covers intelligent vehicle control technology, new energy vehicles, and vehicle dynamic simulation and control.

Renkai Ding was born in Zhenjiang, China, in 1990. He received the Ph.D. degree in vehicle engineering from Jiangsu University, Zhenjiang, China, in 2020.

Since 2020, he has been the Lecturer with Automotive Engineering Research Institute, Jiangsu University, Jiangsu, China. His research interests include vehicle system dynamics, ambient condition perception, and vibration energy regeneration of hybrid electric vehicles.

Qingzhen Han received the Ph.D. degree in automotive engineering from Jiangsu University, Jiangsu, China, in 2018.

He is currently a Lecturer with the School of Mechanical Engineering, Yangzhou University, Jiangsu, China. His main research interests include electric vehicles, vehicle system dynamics, and vibration and noise control technology.

Wenhan Yang was born in Jiangsu, China. He received the B.S. and Ph.D. degrees in mechanical engineering from Chongqing University, Chongqing, China, in 2013 and 2021, respectively.

He is currently a Lecturer with the School of Mechanical Engineering, Yangzhou University, Jiangsu, China. His main research interests include design and manufacture of mechanical parts.